05

The influence of ultrasonic treatment on the microstructure in hot-rolled $(Ni_{54}Fe_{19}Ga_{27})_{99.7}B_{0.3}$ polycrystals

© N.Yu. Surikov[1], E.Yu. Panchenko[1], V.V. Rubanik[2], V.V. Rubanik (jr.)[2], Yu.V. Tsarenko[2], Yu.I. Chumlyakov[1]

[1] National Research Tomsk State University, Tomsk, Russia
[2] Institute of Technical Acoustics of the National Academy of Sciences of Belarus, Vitebsk, Belarus
E-mail: jet_n@mail.ru

Received April 30, 2025
Revised July 16, 2025
Accepted July 16, 2025

The effect of ultrasonic treatment on the microstructure and the potential of ultrasonic treatment to optimize the elastocaloric effect in hot-rolled Heusler $(Ni_{54}Fe_{19}Ga_{27})_{99.7}B_{0.3}$ shape memory alloys were investigated. It was shown that ultrasonic treatment at cryogenic temperatures below the martensitic transformation temperatures leads to the dissolution of $\gamma(\gamma')$-phase particles. Whereas ultrasonic treatment at room temperature does not lead to such effect, but promotes atomic $\gamma-\gamma'$ ordering of secondary phase particles.

Keywords: Heusler alloys, hot rolling, ultrasonic treatment, microstructure, elastocaloric effect.

DOI: 10.61011/TPL.2025.10.62121.20365

Ferromagnetic NiFeGa(B)-based Heusler shape memory alloys have great potential in a wide range of industries. Among the most popular is solid-state cooling, associated with the elastocaloric effect (ECE), as an environmentally friendly alternative to traditional vapor-compression cooling [1–4]. NiFeGa(B) single crystals have high potential for using superelasticity and ECE, but their production on an industrial scale is quite labor-intensive. In polycrystalline materials, there are several problems that complicate their use. Relatively low plasticity of no more than 15–25 % of the set strain at temperatures up to 673 K [5–7] complicates thermomechanical processing and molding of the material. In addition, the incompatibility of the transformation strain of $B2(L2_1)-10M/14M-L1_0$ martensitic transformations (MT) at high values of the crystal anisotropy parameter $A = 2C_{44}/(C_{11}- C_{12}) > 10$ leads to grain boundary cracking, which reduces the cyclic stability of the functional properties of polycrystals [2,6].

In [7–10], a temperature range above 873 K with increased plasticity of NiFeGa(B) alloys by more than 50 % at low deforming stresses of less than 200 MPa was found, and the possibility of hot rolling at temperatures above 873 K with a total strain of up to 50 % without destruction and cracking of the material was shown. The effect of hot rolling on the microstructure features of these alloys was determined. However, during hot rolling, many defects accumulate, a large volume fraction of secondary phases (γ/γ') is precipitate, the volume fraction of material undergoing MT decreases, and residual internal stresses arise. One of the possible methods for controlling the microstructure after significant plastic deformation is ultrasonic treatment (UST). UST allows reducing internal microstresses, modifying the polycrystals texture, and helps to reduce irreversible strain during the MT [11,12]. However, there are very few works on the effect of ultrasound on shape memory alloys and the effect of ultrasonic treatment on the microstructure of NiFeGa(B) alloys has not been studied. Therefore, this work is devoted to the study of the effect of ultrasonic treatment at different temperatures on the microstructure of hot-rolled $(Ni_{54}Fe_{19}Ga_{27})_{99.7}B_{0.3}$ polycrystals with $L2_1(B2)-14M/10M-L1_0$ martensitic transformations.

For the study, $(Ni_{54}Fe_{19}Ga_{27})_{99.7}B_{0.3}$ polycrystals were obtained by arc melting in an argon atmosphere with fivefold remelting. The polycrystals were rolled in four passes with heating before each pass to a temperature above 1073 K. During the pass, the temperature was controlled using a pyrometer and by incandescence color and was strictly above 873 K. The resulting decrease in the plate thickness was 50 %. After rolling, the samples were subjected to ultrasonic treatment at the antinodes of standing stresses wave at a temperature of 77 K for 30 min (UST-77) and at a temperature of 300 K for 15 min (UST-300). The amplitude of alternating stresses was 40 MPa. The UST temperatures were selected based on the different effects of ultrasound on materials with fcc and bcc lattices [12] due to different mechanisms of plastic deformation, as well as differences in the lattices of hot-rolled crystals of $(Ni_{54}Fe_{19}Ga_{27})_{99.7}B_{0.3}$ alloy at UST-77 ($L1_0$-martensite) and UST-300 ($L2_1$-austenite).

The microstructure of the obtained polycrystals was studied by transmission electron microscopy (TEM) on a Hitachi HT-7700 microscope of the Krasnoyarsk Regional Center for Collective Use of the Siberian Branch of the Russian Academy of Sciences. The chemical composition was determined by energy-dispersive X-ray spectroscopy on a Tescan Vega 3 scanning electron microscope. The characteristic temperatures of the start and finish of the direct $(M_s,\ M_f)$ and reverse $(A_s,\ A_f)$ MT and enthalpy change during MT were obtained by the thermoresistance

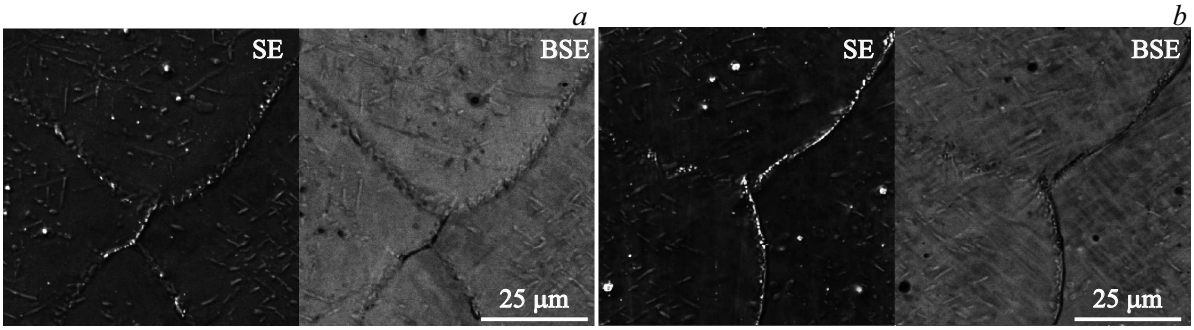

Figure 1. Image of the structure obtained by the secondary electron (SE) and backscattered electron (BSE) detector of $(Ni_{54}Fe_{19}Ga_{27})_{99.7}B_{0.3}$ crystals. *a* — after UST-77, *b* — after UST-300.

Table 1. Average chemical composition of $(Ni_54Fe_{19}Ga_{27})_{99.7}B_{0.3}$ crystals after UST

Treatment	Structure element	Ni, at.%	Fe, at.%	Ga, at.%
UST-77	Matrix	53.4	19.6	27.0
	Particles	54.9	19.2	25.9
UST-300	Matrix	53.1	19.9	27.0
	Particles	59.0	17.3	23.7
γ-phase [8]		54.5	25.6	19.9
γ'-phase [8]		57.3	17.2	25.5

method and differential scanning calorimetry (DSC, Netzsch 404 F1) method with heating and cooling rates of 10 K/min.

According to the chemical analysis (Fig. 1, Table 1), in hot-rolled crystals after UST-77, the particles located along the grain boundaries and in the grain body have a chemical composition close to the matrix. UST-300 leads to a change in the chemical composition of the particles. According to the data from [8] in Table 1, the chemical composition of the particles after UST-300 is closer to the particles of the γ'-phase.

As shown in our previous work [10], hot-rolled crystals contain a specific microstructure: during the rolling process, γ-phase particles are precipitated in the grain body and along the grain boundaries, which contain ordered nanoparticles of the γ'-phase. Despite the fact that rolling was carried out at high temperatures in the austenite phase, residual martensite may arise in the material, presumably due to the high density of defects and thermal stresses. Nevertheless, according to the temperature dependence of electrical resistance, in hot-rolled NiFeGaB crystals before and after UST-77 and UST-300 the MT temperatures are below room temperature (Table 2), while UST leads to a decrease in the MT temperatures.

According to TEM, the UST-77 treatment leads to changes in the microstructure. Residual twinned L10-martensite and a large number of defects were found in the matrix (Fig. 2). The material contains particles of the $\gamma(\gamma')$-phase, including those twinned along the $\{111\}_\gamma$ planes, similar to particles after hot rolling. However, areas of detwinned martensite were found near some particles: in Fig. 2, *a*, the upper microdiffraction pattern corresponds to a γ'-phase particle, and the lower microdiffraction pattern from the area next to the particle corresponds to detwinned $L1_0$-martensite.

In addition, UST-77 leads to the dissolution of $\gamma(\gamma')$-phase particles. In the bright-field images (Fig. 2, *b*–*d*), the preimages of $\gamma(\gamma')$-phase particles are clearly visible, surrounded by dislocations and twinned $L1_0$-martensite. However, the microdiffraction patterns from the particle preimages do not correspond to $\gamma(\gamma')$-phase particles, but correspond to $L1_0$-martensite (the microdiffraction patterns from the matrix and from the region inside the particle preimages are identical). Moreover, in the bright-field images (Fig. 2, *c*, *d*), martensite lamellas intersecting the contour of the particle preimage are clearly visible.

After UST-300, a different microstructure is observed. According to TEM, fragmentation and the degree of twinning along the $\{111\}_\gamma$ plane of secondary phase particles increase significantly (Fig. 3, *a*). Unlike UST-77, no dissolution of $\gamma(\gamma')$-phase particles was detected after UST-300. Based upon the dark-field images in superstructure reflections (Fig. 3, *b*), UST-300 leads to an increase in the volume fraction of the γ'-phase inside the particles up to the complete formation of γ'-phase particles from the γ'-phase, in contrast to nanodispersed inclusions after rolling [10].

The dissolution of $\gamma(\gamma')$-phase particles after UST-77 can be explained as follows. The crystal lattices of $L1_0$-martensite and γ, γ'-phases are close in lattice parameters: $a = 0.381$ nm, $c = 0.327$ nm for the $L1_0$-phase, $a_\gamma = 0.359$ nm for the γ- and γ'-phases [2,13,14]. The difference between the $L1_0$-martensite and $\gamma(\gamma')$-phase

Table 2. MT temperatures of $(Ni_{54}Fe_{19}Ga_{27})_{99.7}B_{0.3}$ crystals

Treatment	M_s, K	M_f, K	A_s, K	A_f, K
Hot-rolling	242	214	232	260
UST-77	235	208	222	254
UST-300	232	208	219	243

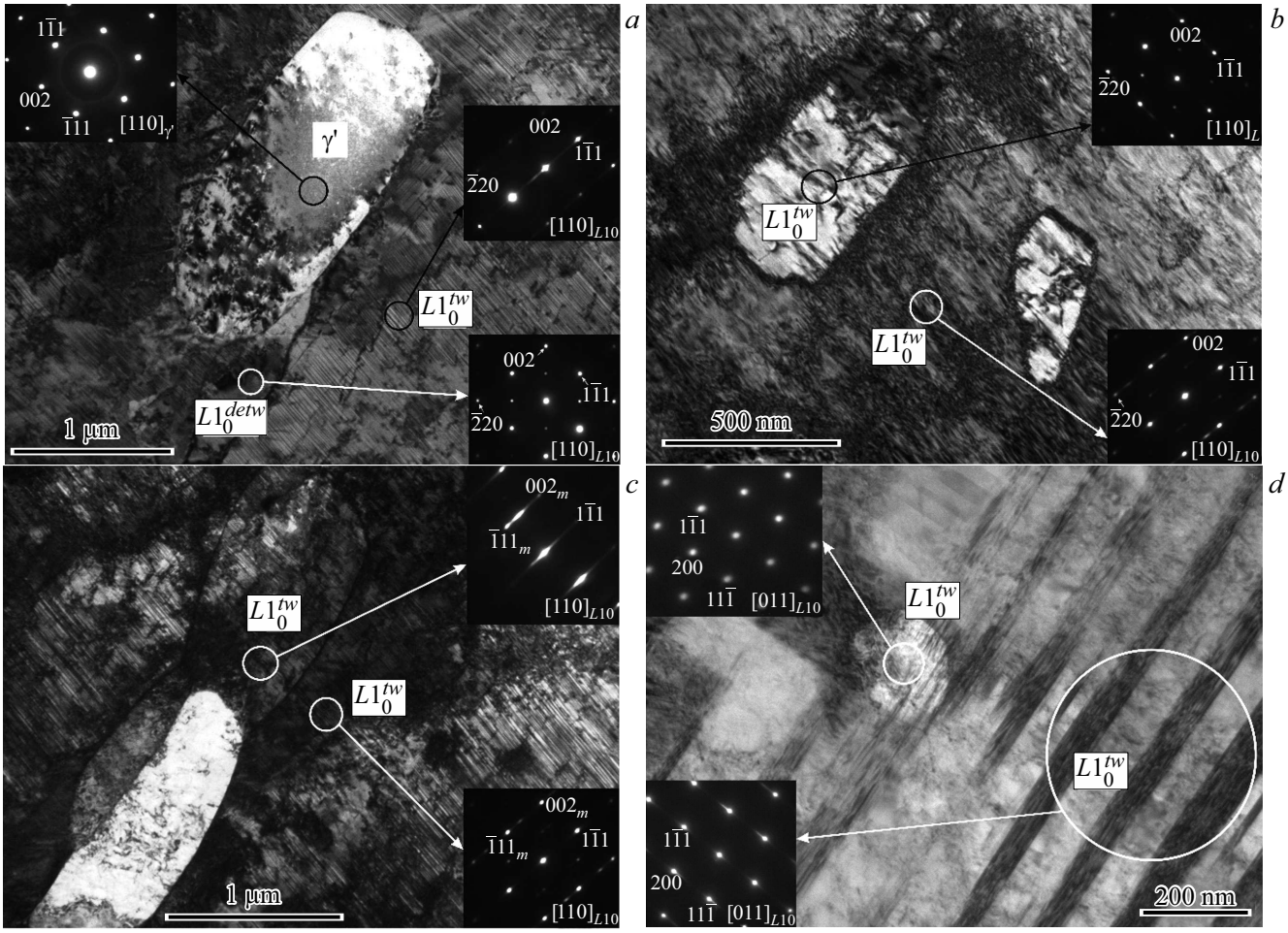

Figure 2. Bright-field images and microdiffraction patterns in the indicated areas corresponding to particles (γ') and twinned/detwinned martensite ($L1_0^{tw}/L1_0^{detw}$) in $(Ni_{54}Fe_{19}Ga_{27})_{99.7}B_{0.3}$ crystals after UST-77.

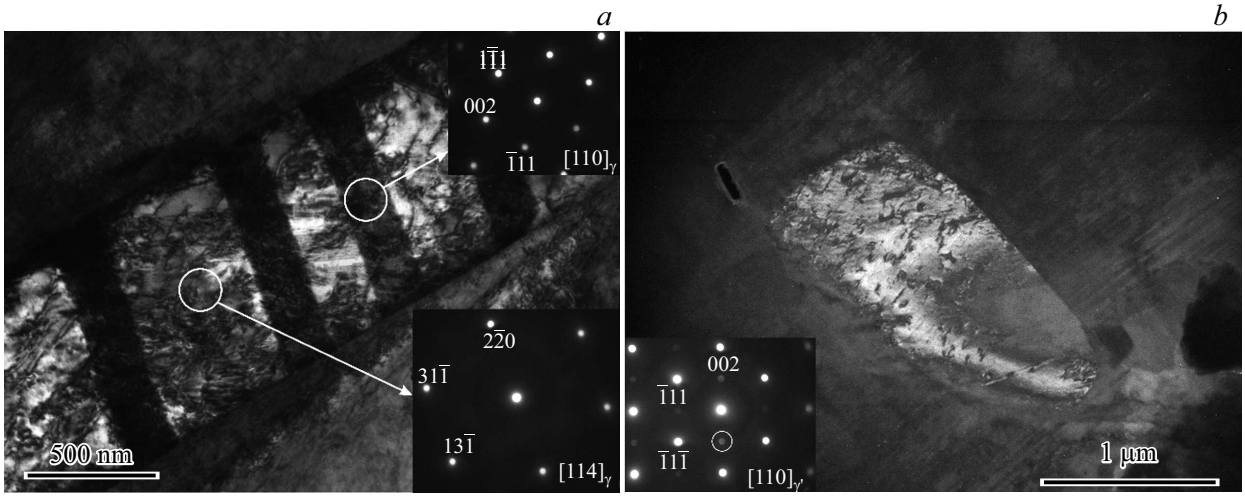

Figure 3. Microstructure of $(Ni_{54}Fe_{19}Ga_{27})_{99.7}B_{0.3}$ crystals after UST-300. *a* — bright-field image of a particle twinned along the $\{111\}_\gamma$ plane and microdiffraction patterns in the areas indicated by circles, *b* — dark-field image of a particle in the superstructure reflection marked in the microdiffraction pattern.

Table 3. MT enthalpy change and the estimated ECE maximum of the $(N_{54}Fe_{19}Ga_{27})_{99}B_{0.3}$ crystals

Treatment	M_s, K	M_f, K	A_s, K	A_f, K	ΔH^{A-M}, J/g	ΔH^{M-A}, J/g	ΔT_{ad}, K
Hot-rolling + annealing (1173 K, 5 min)	253	237	255	268	3.42	2.76	6.1
UST-77 + annealing (1173 K, 5 min)	254	237	253	270	4.57	3.22	7.0
UST-300 + annealing (1173 K, 5 min)	254	236	253	271	4.73	3.14	6.9

lattices does not exceed 8.9 % for any direction, which is significantly less than the lattice deformation at $L2_1-L1_0$ MT, which can reach 13.5 %. In addition, the γ'- and $L1_0$-lattices have the same filling of sublattices with elements of atoms of the same type. Therefore, UST in $L1_0$-martensite can promote strain-induced dissolution of the secondary $\gamma(\gamma')$-phase.

Previously, abnormal strain-induced dissolution of Ni_3Al γ'-intermetallics in the matrix of austenitic Fe−Ni−Al alloys was discovered during high-pressure torsion at cryogenic temperatures up to 77 K [15]. Dissolution of γ'-intermetallics at cryogenic temperatures is associated with the migration of strain-induced interstitial atoms from intermetallic particles into the matrix in the stress field of moving dislocations. With an increase in the deformation temperature, dissolution is replaced by strain-induced precipitation of intermetallics. Based on the above, it can be assumed that, under specified conditions such as multiple cyclic treatments, the dissolution of $\gamma(\gamma')$-phase particles is possible during UST-77 by a similar mechanism. However, this issue requires further research.

During UST-300, firstly, the thermodynamically stable phase is $L2_1(B2)$-austenite. Secondly, diffusion processes are significantly intensified at an elevated UST temperature [12]. Due to the significant difference in the lattices of $L2_1$-austenite ($a_0 = 0.576$ nm [2,14]) and the $\gamma(\gamma')$-phase, the dissolution of particles is impeded. However, inside the particles of the $\gamma(\gamma')$-phase, the process of ordering the γ-phase into the γ'-phase in the field of moving dislocations is possible.

It has been previously shown that, unlike fcc alloys, in bcc alloys UST significantly increases the probability of annihilation of dislocations sliding along different slip planes, which reduces the dislocation density [12,16]. In addition, in bcc alloys UST led to a decrease in the fraction of twin boundaries from 14.6 to 2.7 %. The authors associate this to a decrease in misorientation and subsequent disappearance of twin boundaries due to the motion of dislocations during UST [17]. Therefore, it is possible that a decrease in the defect density in $L2_1(B2)$-austenite (bcc structure) during UST-300 promotes ordering and an increase in the defect density (dislocations and twins) in particles of the $\gamma(\gamma')$-phase with an fcc structure.

After UST, NiFeGaB crystals were briefly heated and cooled to 1173 K at a rate of 20 K/min. After that, the samples were examined by DSC. Annealing leads to an increase in the MT temperatures of all the studied crystals (Tables 2, 3). It is shown that UST leads to an increase in the enthalpy change of direct and reverse MT (ΔH^{A-M} and ΔH^{M-A}) in the annealed crystals (Table 3). This has a positive effect on the potential of NiFeGaB alloys for use in solid-state cooling methods. The value of the specific heat capacity calculated according to the relationship $\Delta T_{ad} \approx \Delta H^{M-A}/C_p$ ($C_p = 455\,\mathrm{J/(kg \cdot K)}$ [10] is the specific heat capacity) [1–6] increases from 6.1 to 7.0 and 6.9 K after UST-77 and UST-300, respectively.

Thus, UST is an effective method for controlling the microstructure of hot-rolled NiFeGaB alloys. UST at cryogenic temperatures in $L1_0$-martensite leads to the dissolution of dispersed particles of the secondary $\gamma(\gamma')$-phase. UST at room temperature in $L2_1(B2)$-austenite promotes an increase in the density of twins in particles and $\gamma - \gamma'$ ordering of particles. UST can also be considered in the context of optimizing the parameters of the elastocaloric effect in the processing of hot-rolled NiFeGaB alloys.

Funding

This research was funded by the Russian Science foundation, project N 23-19-00150 (https://rscf.ru/project/23-19-00150).

Conflict of interest

The authors declare that they have no conflict of interest.

References

[1] E. Villa, C.O. Aguilar-Ortiz, A. Nespoli, P. Álvarez-Alonso, J.P. Camarillo-Garcia, D. Salazar, F. Passaretti, H. Flores-Zúniga, H. Hosoda, V.A. Chernenko, J. Mater. Res. Tech., **8** (5), 4540 (2019). DOI: 10.1016/j.jmrt.2019.07.067

[2] X. Huang, Y. Zhao, H. Yan, N. Jia, B. Yang, Z. Li, Y. Zhang, C. Esling, X. Zhao, Q. Ren, X. Tong, L. Zuo, Scripta Mater., **234**, 115544 (2023). DOI: 10.1016/j.scriptamat.2023.115544

[3] L. Li, Sh. He, F. Xiao, Y. Zeng, Y. Liu, Y. Zhou, X. Cai, X. Jin, Prog. Mater Sci., **153**, 101477 (2025). DOI: 10.1016/j.pmatsci.2025.101477

[4] H. Mevada, B. Liu, L. Gao, Y. Hwang, I. Takeuchi, R. Radermacher, Int. J. Refr., **162**, 86 (2024). DOI: 10.1016/j.ijrefrig.2024.03.014

[5] Y. Xu, B. Lu, W. Sun, A. Yan, J. Liuc, Appl. Phys. Lett., **106**, 201903 (2015). DOI: 10.1063/1.4921531
[6] M. Imran, X. Zhang, M. Qian, L. Geng, Intermetallics, **136**, 107255 (2021). DOI: 10.1016/j.intermet.2021.107255
[7] E.E. Timofeeva, E.Yu. Panchenko, A.S. Eftifeeva, N.Yu. Surikov, A.I. Tagiltsev, I. Kurlevskaya, J. Alloys Compd., **1005**, 176076 (2024). DOI: 10.1016/j.jallcom.2024.176076
[8] A. Biswas, M. Krishnan, Phys. Proc., **10**, 105 (2010). DOI: 10.1016/j.phpro.2010.11.083
[9] A. Biswas, G. Singh, S.K. Sarkar, M. Krishnan, U. Ramamurty, Intermetallics, **54**, 69 (2014). DOI: 10.1016/j.intermet.2014.05.012
[10] N.Y. Surikov, E.Y. Panchenko, I.D. Kurlevskaya, E.I. Yanushonite, A.B. Tokhmetova, Lett. Mater., **14** (4), 306 (2024). DOI: 10.48612/letters/2024-4-306-311
[11] V.V. Rubanik, Jr., V.V. Rubanik, V.V. Klubovich, Mater. Sci. Eng. A, **481**-**482**, 620 (2008). DOI: 10.1016/j.msea.2007.02.134
[12] Q. Cui, X. Liu, W. Wang, S. Tian, V. Rubanik, V. Rubanik, Jr., D. Bahrets, Int. J. Miner. Met. Mater., **31**, 1322 (2024). DOI: 10.1007/s12613-023-2745-z
[13] A.F. Manchón-Gordón, J.J. Ipus, M. Kowalczyk, J.S. Blázqueza, C.F. Conde, P. Švec, T. Kulik, A. Conde, J. Alloys Compd., **889**, 161819 (2021). DOI: 10.1016/j.jallcom.2021.161819
[14] E. Panchenko, E. Timofeeva, A. Eftifeeva, K. Osipovich, N. Surikov, Y. Chumlyakov, G. Gerstein, H. Maier, Scripta Mater., **162**, 387 (2019). DOI: 10.1016/j.scriptamat.2018.12.003
[15] V.V. Sagaradze, V.A. Shabashov, N.V. Kataeva, K.A. Kozlov, A.R. Kuznetsov, A.V. Litvinov, Mater. Lett., **172**, 207 (2016). DOI: 10.1016/j.matlet.2015.11.078
[16] J. Wang, X.F. He, H. Cao, L.X. Jia, Y.K. Dou, W. Yang, Acta Phys. Sin., **70** (6), 068701 (2021). DOI: 10.7498/aps.70.20201659
[17] M. Zohrevand, M. Aghaie-Khafri, F. Forouzan, E. Vuorinen, Ultrasonics, **116**, 106519 (2021). DOI: 10.1016/j.ultras.2021.106519